KMT9 Controls Stemness and Growth of Colorectal Cancer

Christopher Berlin[1,2], Félicie Cottard[3], Dominica Willmann[3], Sylvia Urban[3], Stephan M. Tirier[4,5], Lisa Marx[1], Karsten Rippe[4,5], Mark Schmitt[6], Valentina Petrocelli[6], Florian R. Greten[6,7,8], Stefan Fichtner-Feigl[1], Rebecca Kesselring[1], Eric Metzger[3,9], and Roland Schüle[3,9]

ABSTRACT

Colorectal cancer is among the leading causes of cancer-associated deaths worldwide. Treatment failure and tumor recurrence due to survival of therapy-resistant cancer stem/initiating cells represent major clinical issues to overcome. In this study, we identified lysine methyltransferase 9 (KMT9), an obligate hetero-dimer composed of KMT9α and KMT9β that monomethylates histone H4 at lysine 12 (H4K12me1), as an important regulator in colorectal tumorigenesis. KMT9α and KMT9β were overexpressed in colorectal cancer and colocalized with H4K12me1 at promoters of target genes involved in the regulation of proliferation. Ablation of KMT9α drastically reduced colorectal tumorigenesis in mice and prevented the growth of murine as

well as human patient-derived tumor organoids. Moreover, loss of KMT9α impaired the maintenance and function of colorectal cancer stem/initiating cells and induced apoptosis specifically in this cellular compartment. Together, these data suggest that KMT9 is an important regulator of colorectal carcinogenesis, identifying KMT9 as a promising therapeutic target for the treatment of colorectal cancer.

Significance: The H4K12 methyltransferase KMT9 regulates tumor cell proliferation and stemness in colorectal cancer, indicating that targeting KMT9 could be a useful approach for preventing and treating this disease.

Introduction

Colorectal cancer, which includes hereditary, sporadic, and colitis-associated forms, is one of the leading causes of cancer-associated deaths worldwide (1). Four distinct consensus molecular colorectal cancer subtypes (CMS1–4) have been defined based on gene expression signatures, DNA methylation status, somatic copy number alterations, miRNA regulation changes, and presence of genetic aberrations in tumor suppressor genes [e.g., tumor protein p53 (*TP53*), adenomatous polyposis coli protein (*APC*)] or oncogenes [e.g., kristen rat sarcoma viral oncogenes (*KRAS*); refs. 2–6]. To date, systemic therapeutic options for colorectal cancer include chemotherapy (adju-

vant and neoadjuvant) and to a lesser extent, therapeutic antibodies directed against growth factor receptors, for example, vascular endothelial growth factor receptor (VEGFR; ref. 7). Despite treatment, 30% to 40% of human patients relapse and suffer from tumor recurrence (8). This has been attributed to the acquirement of genetic aberrations during therapy and survival of cancer stem/initiating cells (CSC; ref. 9). CSCs and adult intestinal stem cells in the healthy gut have similar characteristics with respect to their self-renewal and differentiation capacity (10). For example, leucine-rich repeat containing g-protein–coupled receptor 5 (*LGR5*), a well-established target of the *WNT* signalling pathway, is expressed in benign intestinal stem cells and also defined as a CSC marker because *LGR5*-expressing (*LGR5*^{+}) tumor cells have a high clonogenic capacity (11–13). Currently, resistant CSC populations are poorly characterized and therapeutic strategies for targeting CSCs remain to be identified (14, 15). One important feature of CSCs is their dynamic ability to switch between proliferative or differentiated states by modulating gene expression, which suggests the existence of epigenetic regulation (16).

Histone methyltransferases (HMT) catalyze the transfer of a methyl group from S-adenosyl-methionine (SAM) to lysine or arginine residues of histones. Histone methylation regulates various biological processes including proliferation, cell cycle, and stemness (17). Aberrant expression of histone methytransferases contributes to global changes of the histone methylation landscape, which has been associated with colorectal cancer development, progression, and patient survival (18). Therefore, targeting epigenetic regulators such as HMTs has been proposed as therapeutic strategy for colorectal cancer (19–21).

Recently, we identified the novel histone lysine methyltransferase KMT9 (22). KMT9 functions as an obligatory heterodimer composed of KMT9α (also named N6AMT1) and KMT9β (also named TRMT112), and their interaction is required for SAM binding and methyltransferase activity (22). KMT9 monomethylates lysine 12 of histone H4 (H4K12me1), thereby controlling genes that regulate proliferation of prostate and lung cancer cells (22, 23). Of note, high levels of KMT9 have been associated with poor patient survival in

[1]Klinik für Allgemein- und Viszeralchirurgie, Klinikum der Albert-Ludwigs-Universität Freiburg, Freiburg, Germany. [2]IMM-PACT Clinician Scientist Program, Medizinische Fakultät, Universität Freiburg, Freiburg, Germany. [3]Klinik für Urologie und Zentrale Klinische Forschung, Klinikum der Albert-Ludwigs-Universität Freiburg, Freiburg, Germany. [4]German Cancer Research Center (DKFZ) & Bioquant, Division of Chromatin Networks, Heidelberg, Germany. [5]Deutsches Konsortium für Translationale Krebsforschung, Heidelberg, Germany. [6]Institut für Tumorbiologie und experimentelle Therapie, Georg-Speyer-Haus Frankfurt/Mainz, Germany. [7]Frankfurt Cancer Institute, Goethe Universität Frankfurt, Frankfurt/Mainz, Germany. [8]Deutsches Konsortium für Translationale Krebsforschung, Frankfurt/Mainz Germany. [9]Deutsches Konsortium für Translationale Krebsforschung, Freiburg, Germany.

C. Berlin and F. Cottard contributed equally to this article.

Corresponding Author: Roland Schüle, Klinik für Urologie und Zentrale Klinische Forschung, Albert-Ludwigs-Universität Freiburg, Breisacherstrasse 66, Freiburg 79106, Germany. Phone: 4976-1270-63100; Fax: 4976-1270-63110; E-mail: roland.schuele@uniklinik-freiburg.de

prostate and lung cancer (22, 23). Here, we investigated the function of KMT9 in colorectal cancer *in vitro* in human and murine organoid systems, as well as *in vivo* in murine models of colorectal cancer. Our data demonstrate that KMT9 is an essential regulator of colorectal cancer cell proliferation and stemness, which establishes KMT9 as a potential therapeutic target for colorectal cancer.

Materials and Methods

Plasmids

pLenti6-miKMT9α was constructed by inserting the DNA sequence corresponding to a miRNA against human KMT9α into pLenti6/V5-DEST according to the manufacturer's instructions (Life Technologies). Cloning details can be obtained upon request. Details regarding the miRNA sequences used for the cloning can be found in the Supplementary Table S1.

The Cancer Genomes Atlas data analysis

Normalized The Cancer Genomes Atlas (TCGA) gene expression data were downloaded with TCGA-Assembler Version 2.0 (https://github.com/compgenome365/TCGA-Assembler-2;.rsem.genes.normalized_results) and CMS classification of human colorectal cancer samples was calculated using CMScaller, a package in R, as described previously (24).

Mouse studies

$Apc^{fl/fl}$ $p53^{fl/fl}$ $Kras^{G12D/+}$ $Kmt9α^{fl/fl}$, $Apc^{fl/fl}$ $p53^{fl/fl}$ $Kras^{G12D/+}$ $Kmt9α^{+/+}$, Rosa26-CreERT2x$Kmt9α^{wt/wt}$ ($Kmt9α^{wt/wt}$), Rosa26-CreERT2x$Kmt9α^{fl/fl}$ ($Kmt9α^{ind-fl/fl}$), Villin1 (Vil1)-CreERT2x$Kmt9α^{wt/wt}$ ($Kmt9α^{IEC-wt/wt}$), Villin1 (Vil1)-CreERT2x$Kmt9α^{fl/fl}$ ($Kmt9α^{IEC-fl/fl}$) mice were used for organoids generation and *in vivo* experiments. The mice were maintained in a temperature- and humidity-controlled animal facility with a 12-hour light/dark cycle and free access to water. Animals were sacrificed using cervical dislocation and tissues were immediately collected for further experiments.

Azoxymethane/dextran sodium sulfate treatment

$Kmt9α^{wt/wt}$, $Kmt9α^{ind-fl/fl}$, $Kmt9α^{IEC-wt/wt}$, and $Kmt9α^{IEC-fl/fl}$ mice between 10 and 12 weeks of age were given an intraperitoneal injection of 10 mg/kg body weight of azoxymethane (AOM; Sigma). Each experiment was conducted using 24 mice from different litters [$n = 12$ control mice ($Kmt9α^{wt/wt}$/$Kmt9α^{IEC-wt/wt}$) and $n = 12$ $Kmt9α^{ind-fl/fl}$ or $Kmt9α^{IEC-fl/fl}$ mice]. One week after the first intraperitoneal AOM injection, animals were given *ab libitum* access to drinking water with 1.25% dextran sodium sulfate (DSS; MP Biomedicals) for seven days followed by another seven days of normal drinking water, for a total of 5 cycles. A second intraperitoneal AOM injection was given after the first cycle. For *in vivo* investigation of KMT9α, mice were injected with 1 mg of tamoxifen for five days and fed with tamoxifen containing food during the entire procedure. Body weight was measured once a week. Following the last cycle of normal drinking water, mice were sacrificed using cervical dislocation. Tumors were measured with a caliper and tumor volume was calculated by the formula $V = 4/3 \times 3.142 \times ((\text{width}+\text{length})/4)^3$. Tumors were fixed in 10% formalin for subsequent embedding or alternatively frozen in liquid nitrogen for subsequent analyses.

Organoid isolation

For establishment of healthy colon organoids, colonic crypts of C57BL/6 mice were isolated as described previously (25). For generation of APKK ($Apc^{KO}/Kras^{G12D}/p53^{KO}/Kmt9α^{KO}$) and APK ($Apc^{KO}/Kras^{G12D}/p53^{KO}$) organoids, colonic crypt of $Apc^{fl/fl}$ $p53^{fl/fl}$ $Kras^{G12D/+}$ $Kmt9α^{fl/fl}$, and $Apc^{fl/fl}$ $p53^{fl/fl}$ $Kras^{G12D/+}$ $Kmt9α^{+/+}$ mice were isolated as described previously (25). The deletion of the floxed sequences was mediated by infection with Cre-expressing adenovirus (BioCat GmbH). For generation of AOM/DSS tumor organoids, colonic tumors were excised from $Kmt9α^{wt/wt}$ or $Kmt9α^{ind-fl/fl}$ mice after AOM/DSS treatment. Tumor tissue was manually dissected and a single-cell suspension containing tumor stem cells was generated using the Tumour Dissociation Kit, mouse (Miltenyi Biotec) according to the manufacturer's protocol. Patient-derived organoids (PDO) were isolated from human colorectal cancer tissue using Tumor Dissociation Kit, human (Miltenyi Biotec) according to the manufacturer's protocol. The single cells obtained were resuspended in a solution containing growth factor-reduced Matrigel (Corning) and Advanced DMEM-F12 medium (Thermo Fisher Scientific) in a 1:1 ratio. For each dome, approximately 1,000 cells were seeded in a 50 μL drop of Matrigel/Advanced DMEM-F12 in 24-well plates. The Matrigel was allowed to polymerize at 37°C for 20 minutes and then covered with 600 μL of culture medium.

Organoid culture

Healthy colon organoids and colorectal cancer PDOs were maintained in IntestiCult Organoid Growth Medium [Stemcell Technologies, catalog #06005 (for mouse organoids) and catalog #06010 (for human organoids)] supplemented with penicillin/streptomycin. Mouse tumor organoids were maintained in basal medium [Advanced DMEM-F12 supplemented with penicillin/streptomycin, HEPES 10 mmol/L (Invitrogen), Glutamax 1× (Invitrogen), N2 1× (Gibco), B27 1× (Gibco), and N-acetylcysteine 1 mmol/L (Sigma)]. For AOM/DSS tumor organoids, the basal medium was supplemented with 50 ng/mL EGF (Peprotech). After 3 to 5 passages, the organoids were frozen and cryopreserved as stocks for future experiments. In general, the organoids were used between passage numbers 7 and 15. For *in vitro* deletion of *Kmt9α*, AOM/DSS tumors organoids were treated with 1 μmol/L 4-hydroxytamoxifen or EtOH (vehicle) as a control. Mouse and human organoids were subcultured in Matrigel every 5–7 days or every 14 days, respectively.

Chromatin immunoprecipitation and sequencing

Chromatin immunoprecipitation (ChIP) experiments were performed as previously described (26). Two days after seeding, AOM/DSS tumor organoids were incubated with 1 μmol/L tamoxifen or EtOH (vehicle) as a control. Five days after tamoxifen incubation, organoids were dissociated into single-cell suspension using TrypLE (Gibco). Cell pellets were washed twice with cold PBS, cross-linked with 1% PFA for 15 minutes at 4°C, and then rinsed twice with ice-cold PBS. The pellets were resuspended in TSE I buffer (20 mmol/L Tris-HCL pH 8, 2 mmol/L EDTA, 150 mmol/L NaCL, 0.1% SDS, and 1% Triton X-100) and sonicated for 1 hour at 4°C (Bioruptor, Diagenode). Immunoprecipitation was performed with GammaBind G-Sepharose beads (GE-Healthcare) and specific antibodies for anti-KMT9α (#27630, lot 20062017, Schüle Lab); anti-H4K12me1 (#27429, lot 27062017, Schüle Lab); anti-KMT9β (#28358, lot 03042018, Schüle Lab). Libraries were prepared from immunoprecipitated DNA according to standard methods. ChIP sequencing (ChIP-seq) libraries were sequenced using a HiSeq 2000 (Illumina) at the sequencing core facility of the MPI-IE, Freiburg. Reads were aligned to the mm10 build of the mouse genome using Bowtie 2 (RRID:SCR_016368; ref. 27). Data were further analyzed using the peak finding algorithm MACS 1.42 (28) using input as control. All peaks with FDR greater than 2.0% were

excluded from further analysis. The reads were used to generate the genome-wide intensity profiles, which were visualized using the IGV genome browser (29). HOMER (RRID:SCR_010881; ref. 30) was used to annotate peaks (annotatePeaks.pl) and to calculate overlaps between different peak files (mergePeaks). The genomic features (promoter, exon, intron, 3′UTR, and intergenic regions) were defined using Refseq (RRID:SCR_003496). Seqplots (https://github.com/Przemol/seqplots) was used to visualize the signals in heatmaps. Data are deposited under GSE150506.

Single-cell mRNA sequencing

Two days after seeding, Kmt9α$^{ind-fl/fl}$ AOM/DSS tumor organoids were treated with 1 μmol/L tamoxifen or EtOH (vehicle) as a control. Five days later, the organoids were dissociated into single-cell suspensions using TrypLE for 20 minutes at 37°C. After dissociation, single-cell suspensions were washed twice in PBS, centrifuged for 5 minutes at $300 \times g$, and counted using a LUNA automated cell counter (Logos Biosystems). Single cell capture, reverse transcription, and library preparation were carried out on the Chromium platform (10× Genomics) with the single-cell 3′ reagent v2 protocol according to the manufacturer's recommendations using 1×10^4 cells as input per reaction well. The two final libraries [tamoxifen/EtOH (vehicle)] were pooled and sequenced on two Illumina NovaSeq SP lanes (paired-end 26 bp + 96 bp). Raw sequencing data were processed and aligned to the mouse genome (mm10) using the CellRanger pipeline (10x Genomics version 3.1, SCR_017344). Data are deposited under GSE150506. Previously published single-cell mRNA sequencing (scRNA-seq) data from 23 Korean patients with colorectal cancer (GSE132435) were analyzed using Seurat v3 as described above (31). Details regarding the analysis of scRNA-seq data can be found in the Supplementary Materials and Methods.

RNA sequencing

RNA from AOM/DSS organoids treated with tamoxifen or EtOH (vehicle), APK and APKK tumor organoids, miCtrl or miKMT9α transduced-PDO organoids, and normal colonic epithelial cells was isolated using RNeasy Mini columns (Qiagen). Total RNA from KMT9α-proficient and -deficient AOM/DSS tumors ($n = 5$ for each group) was isolated using TRIzol (Invitrogen). RNA samples were sequenced by the standard Illumina protocol to create raw sequence files (.fastq files) at Novogene, London. Reads were aligned to the mm10 build of the mouse genome using STAR version 2.7 (RRID: SCR_004463; ref. 32). The aligned reads were counted with HOMER software (RRID:SCR_010881; analyzeRepeats) and differentially expressed genes were identified using EdgeR (RRID:SCR_012802; ref. 33). RNA sequencing (RNA-seq) experiments from tumor organoids were performed in biological triplicates. P values $<10^{-6}$ were considered as statistically significant. For transcriptome analyses from whole-tumor tissue of AOM/DSS tumors, the 3,000 most significantly deregulated transcripts (2,306 genes) were used to perform gene set enrichment analyses (GSEA; RRID:SCR_003199). Data are deposited under GSE150506.

Protein isolation and Western blot analysis

Fresh-frozen human tumor and adjacent healthy colonic tissue were provided by the Ontario Tumour Bank, which is supported by the Ontario Institute for Cancer Research through funding provided by the Government of Ontario. Tissue was kept on ice and manually dissected and minced for subsequent RIPA lysis. For total protein isolation from organoids, Matrigel-cultured organoids were harvested using TrypLE to break up the domes and were washed with PBS. Organoids and human tissue were lysed in ice-cold RIPA buffer (1 mmol/L EDTA, 50 mmol/L Tris-HCl pH7.5, 0.1% SDS, 150 mmol/L NaCl, 1% NP-40, 1% sodium deoxycholate) containing complete EDTA-free Protease Inhibitor Cocktail (Roche) for 10 minutes on ice. After centrifugation for 10 minutes at 13,000 rpm at 4°C, supernatant was collected and protein concentration was determined using Bradford assay. The list of the antibodies used for Western blot analysis can be found in the Supplementary Materials and Methods.

Study approvals

Experimental mice were housed in the pathogen-free barrier facility of the University Medical Center Freiburg in accordance with institutional guidelines and all experiments were approved by the regional board.

Human tumor organoids were established at Georg-Speyer-Haus from fresh human tumor tissue according to regional regulations and the experiments were approved by the regional ethics committee (Ethikkommission Universitätsklinikum Frankfurt/Main 274/18). Informed consent was obtained from all donors of tissue.

Statistical analysis

Data are represented as mean ± SEM. Significance was calculated by two-tailed Student t test, by one-way ANOVA, and Tukey multiple comparisons test as indicated in the figure legends. Statistical significance was set to $P < 0.05$ and is represented as following: ****, $P < 0.0001$; ***, $P < 0.001$; **, $P < 0.01$; *, $P < 0.05$; ns, not significant. Sample sizes are indicated where appropriate.

Additional methods

Additional methods including virus production and organoid transduction, organoid size assessment, colonic epithelial cells isolation, core histone isolation, list of the antibodies used for Western blot analysis, cell proliferation assay, flow cytometry, quantitative RT-PCR analysis, scRNA-seq, hematoxylin and eosin, and immunohistochemical staining and TUNEL assay can be found in the Supplementary Materials and Methods.

Data availability statement

To ensure data availability, all RNA-seq, scRNA-seq, and ChIP-seq data have been deposited at GEO under GSE150506. All data that support the findings of this study are available from the corresponding authors upon reasonable request without any restrictions.

Availability of materials

All unique materials are readily available from the authors without any restrictions.

Results

Colorectal tumorigenesis is modulated by KMT9α

To investigate whether KMT9 plays a functional role in colorectal cancer, we profiled *KMT9α* and *KMT9β* mRNA expression in healthy human colon and primary colon adenocarcinoma tissues. A large cohort TCGA (34) of 256 patients with colorectal cancer revealed a significant increase in both *KMT9α* and *KMT9β* mRNA in colorectal cancer tissue compared with healthy colon (**Fig. 1A** and **B**). CMS stratification revealed significant overexpression of *KMT9α* in CMS2-, CMS3-, and CMS4- but not in CMS1-tumors, whereas *KMT9β* mRNA was significantly increased in all subtypes (Supplementary Fig. S1A–S1C). Moreover, Western blot analyses showed that both KMT9α and KMT9β protein levels were strongly increased in human colorectal
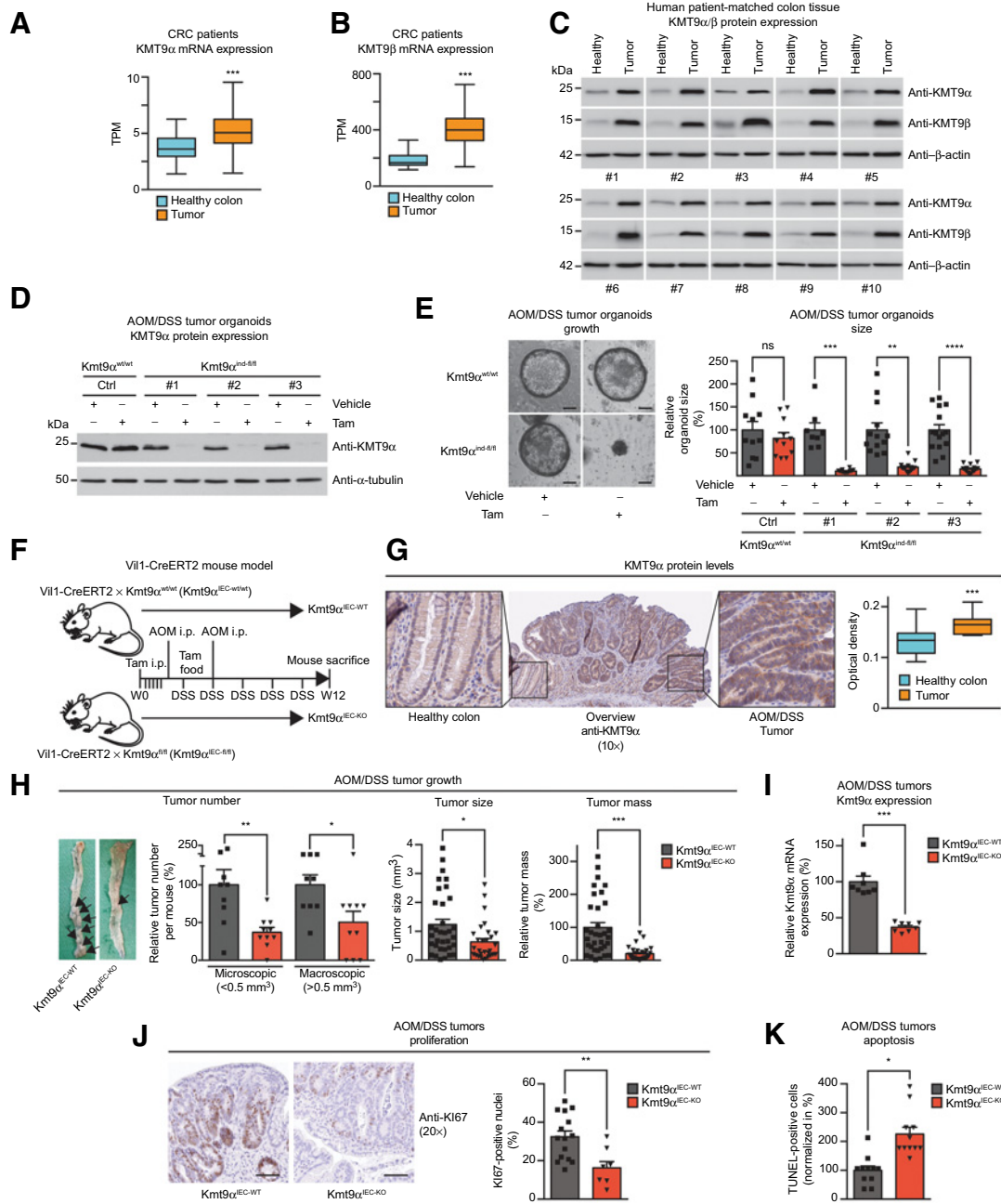
Figure 1.
Colorectal tumorigenesis is modulated by KMT9α. **A** and **B,** *KMT9α* (**A**) and *KMT9β* (**B**) mRNA expression in healthy human colon ($n = 39$) and colon adenocarcinoma ($n = 217$) from patients with colorectal cancer. Data were retrieved from TCGA database. **C,** Western blot showing the expression of KMT9α and KMT9β in human colorectal cancer tumors and patient-matched healthy colon tissue. **D,** Western blot showing tamoxifen (Tam)–dependent deletion of KMT9α in three individual (#1, #2, and #3) AOM/DSS tumor organoid cultures, where control (Ctrl) AOM/DSS tumor organoids showed no KMT9α loss. **E,** Representative images of Kmt9α$^{wt/wt}$ and Kmt9α$^{ind-fl/fl}$ AOM/DSS tumor organoids (#3) cultured in the presence of vehicle or tamoxifen for 7 days. Scale bars, 50 µm (left). Right, relative size of tumor organoids cultured in the presence of vehicle or tamoxifen. **F,** Schematic summarizing the treatment course of Kmt9α$^{IEC-wt/wt}$ and Kmt9α$^{IEC-fl/fl}$ mice with AOM and DSS to induce inflammation-associated tumors. KMT9α deletion in Kmt9α^{IEC-KO} mice was induced with tamoxifen. Kmt9α^{IEC-WT} mice treated with tamoxifen served as controls. **G,** KMT9α protein levels in healthy murine colon ($n = 11$) and AOM/DSS tumors ($n = 11$) of Kmt9α^{IEC-WT} mice are shown by immunohistochemistry (left) and quantification of the data (right). **H,** Representative images showing fewer tumors (black arrowheads) in the colon of Kmt9α^{IEC-KO} mice compared with Kmt9α^{IEC-WT} mice. Graphs show the incidence of microscopic (<0.5 mm^3) and macroscopic (>0.5 mm^3) tumors (left), tumor size (middle), and relative tumor mass (right) for Kmt9α^{IEC-WT} ($n = 9$) and Kmt9α^{IEC-KO} ($n = 10$) mice. **I,** Intratumoral expression of *Kmt9α* mRNA was analyzed by qRT-PCR from AOM/DSS tumors of Kmt9α^{IEC-WT} and Kmt9α^{IEC-KO} mice ($n = 8$ tumors/group). **J,** Immunohistochemical staining of proliferation marker Ki67 in Kmt9α^{IEC-WT} and Kmt9α^{IEC-KO} AOM/DSS tumors (left) and quantification of the percentage of Ki67-positive nuclei (right). Scale bars, 100 µm, $n = 15$ (Kmt9α^{IEC-WT}) and $n = 7$ (Kmt9α^{IEC-KO}) AOM/DSS tumors. **K,** TUNEL staining showing apoptosis in Kmt9α^{IEC-KO} AOM/DSS tumors in comparison with Kmt9α^{IEC-WT} control tumors ($n = 11$ tumors/group). All data represent means ± SEM; *, $P < 0.05$; **, $P < 0.01$; ***, $P < 0.001$; ****, $P < 0.0001$; two-tailed Student t test. CRC, colorectal cancer.

cancer tissue compared with patient-matched healthy colon (**Fig. 1C**). We therefore hypothesized that KMT9 might play a functional role in colorectal tumorigenesis.

Because KMT9α is indispensable for KMT9's histone methyltransferase activity (22), we engineered mice with conditional *Kmt9α* alleles by flanking exon 2 and 3 with loxP sites (Kmt9$\alpha^{fl/fl}$) to unravel potential functions of KMT9 in colorectal tumorigenesis. For initial experiments, Kmt9$\alpha^{fl/fl}$ mice were crossed to the Rosa26-CreERT2 deleter strain (35) to produce Kmt9$\alpha^{ind-fl/fl}$ mice for tamoxifen-inducible deletion of *Kmt9α*. Crosses of mice with *Kmt9α* wild-type (wt) alleles to Rosa26-CreERT2 mice, referred to as Kmt9$\alpha^{wt/wt}$, served as controls. We treated Kmt9$\alpha^{ind-fl/fl}$ and Kmt9$\alpha^{wt/wt}$ mice with AOM and DSS to induce inflammatory colorectal tumor growth (36, 37) and established three-dimensional (3D) epithelial organoid cultures from AOM/DSS–associated tumors (Supplementary Fig. S1D). In the absence of tamoxifen treatment, KMT9α and KMT9β protein levels were increased in four independent AOM/DSS tumor organoids from Kmt9$\alpha^{wt/wt}$ (Ctrl) and Kmt9$\alpha^{ind-fl/fl}$ (#1, #2, #3) mice compared with healthy colon organoids (Supplementary Fig. S1E). This increase is in accordance with observations we made in human patient samples (**Fig. 1A–C**). Following tamoxifen treatment, KMT9α protein was efficiently depleted in the three independent Kmt9$\alpha^{ind-fl/fl}$ AOM/DSS tumor organoids compared with control Kmt9$\alpha^{wt/wt}$ AOM/DSS tumor organoids (**Fig. 1D**). Importantly, upon loss of KMT9α, AOM/DSS tumor organoids displayed a shrinkage in size (**Fig. 1E**), and the proliferation rate was strongly decreased (Supplementary Fig. S1F).

To investigate whether KMT9α loss affects tumor formation and growth *in vivo*, Kmt9$\alpha^{fl/fl}$ mice were crossed to the Villin1 (Vil1)-CreERT2 deleter strain (38), which allows tamoxifen-inducible deletion of *Kmt9α* specifically in intestinal epithelial cells (IEC) of Kmt9$\alpha^{IEC-fl/fl}$ mice (**Fig. 1F**). Tamoxifen-treated Kmt9$\alpha^{IEC-fl/fl}$ mice were compared with tamoxifen-treated Kmt9$\alpha^{IEC-wt/wt}$ mice (hereafter termed Kmt9α^{IEC-KO} and Kmt9α^{IEC-WT}, respectively). Upon AOM/DSS treatment, Kmt9α^{IEC-WT} mice developed colorectal tumors as expected (36, 37). Immunohistochemical and qRT-PCR analyses of the tumors observed in Kmt9α^{IEC-WT} mice revealed a significant increase in KMT9α mRNA and protein levels in AOM/DSS tumors compared with adjacent healthy tissue (**Fig. 1G**; Supplementary Fig. S1G). In contrast to Kmt9α^{IEC-WT} mice, Kmt9α^{IEC-KO} animals displayed a dramatic decrease in tumor burden characterized by a reduced number of microscopic and macroscopic colon tumors per mouse as well as a significantly smaller tumor size and mass (**Fig. 1H**). The few small tumors found in Kmt9α^{IEC-KO} mice displayed reduced *Kmt9α* expression in comparison with tumors in Kmt9α^{IEC-WT} mice (**Fig. 1I**). Analysis of cell proliferation and apoptosis showed that KMT9α-depleted tumors had reduced levels of proliferation marker KI67 (**Fig. 1J**) and increased apoptotic activity (**Fig. 1K**). In the absence of AOM/DSS treatment, colon tissue from Kmt9α^{IEC-KO} and Kmt9α^{IEC-WT} mice did not show any apparent morphologic differences (Supplementary Fig. S1H and S1I). Moreover, proliferation analysis of healthy colon crypts by KI67 staining did not reveal any significant differences between Kmt9α^{IEC-WT} and Kmt9α^{IEC-KO} mice without AOM/DSS treatment (Supplementary Fig. S1J). More importantly, transcriptome analysis performed on purified epithelial colon cells from AOM/DSS treatment-naïve Kmt9α^{IEC-WT} and Kmt9α^{IEC-KO} mice revealed only 12 significantly differentially expressed genes in KMT9α-deficient compared with KMT9α-proficient colon, thereby emphasizing the specific role of KMT9α in colorectal tumor tissue (Supplementary Table S2). Together, these data demonstrate that inflammation-associated colorectal tumorigenesis in mice is controlled by KMT9α.

KMT9α controls the expression of cell-cycle genes in AOM/DSS tumors and organoids

To gain mechanistic insight into KMT9α-mediated gene regulation, we determined the transcriptomes of vehicle- and tamoxifen-treated Kmt9$\alpha^{ind-fl/fl}$ AOM/DSS tumor organoids by RNA-seq. The intersection of the differentially expressed gene sets for the three Kmt9$\alpha^{ind-fl/fl}$ tumor organoids revealed a common pool of 1,183 KMT9α-dependent genes (**Fig. 2A**). GSEA for these 1,183 genes uncovered terms associated with "cell cycle" and "apoptosis" as significantly deregulated biological processes (**Fig. 2B**). Accordingly, we found a significant downregulation of numerous genes involved in cell-cycle control in KMT9α-depleted AOM/DSS tumor organoids (**Fig. 2C**). qRT-PCR analysis validated reduced expression of cell-cycle regulators such as aurora kinase b (*Aurkb*), e2f transcription factor 1 (*E2f1*), establishment of sister chromatid cohesion N-acetyltransferase 2 (*Esco2*), minichromosome maintenance complex component 6 (*Mcm6*), pcna clamp associated factor (*Pclaf*), proline rich 11 (*Prr11*), rad51 paralog c (*Rad51c*), replication protein a2 (*Rpa2*), and dna topoisomerase II alpha (*Top2a*) upon KMT9α loss (Supplementary Fig. S2A). To validate these findings, we analyzed whether KMT9α depletion in AOM/DSS tumor organoids resulted in changes to the cell-cycle phase distribution by flow cytometry. KMT9 depletion was associated with an increase in G_0–G_1 cells and a reduction of the S-phase population (**Fig. 2D**), which suggests that loss of KMT9 decreased cell proliferation. Importantly, these analyses also revealed an early apoptotic sub-G_0 population in the KMT9α-depleted tumor organoids, which is consistent with our *in vivo* findings (**Fig. 1K**). Analysis of the representative AOM/DSS tumor organoids #3 uncovered significant upregulation of proapoptotic genes upon KMT9α depletion (Supplementary Fig. S2B). Upregulation of genes such as phorbol-12-myristate-13-acetate-induced protein 1 (*Pmaip1*) and transforming growth factor beta 2 (*Tgfb2*) was verified by qRT-PCR (Supplementary Fig. S2C). Further supporting the notion that KMT9α depletion promotes apoptosis of AOM/DSS tumor organoids, we detected an increase in cleaved caspase-3 levels (Supplementary Fig. S2D) and in Annexin V–positive (Annexin V$^+$) and DAPI-negative (DAPI$^-$) apoptotic cells (Supplementary Fig. S2E) upon loss of KMT9α. Because KMT9 writes the H4K12me1 histone mark, we asked whether ablation of KMT9α resulted in decreased H4K12me1 levels. Western blot analyses showed a strong decrease in H4K12me1 in KMT9α-depleted AOM/DSS tumor organoids #3 (Supplementary Fig. S2F). To investigate whether the differentially regulated cell-cycle genes identified were direct KMT9 target genes, we analyzed the genomic localization of KMT9α, KMT9β, and H4K12me1 by ChIP-seq in AOM/DSS tumor organoids #3. We uncovered 5,652 KMT9α, KMT9β, and H4K12me1 colocalizations (**Fig. 2E**) that were enriched around the transcription start site (TSS) of target genes (**Fig. 2F**). In total, we observed the presence of KMT9α, KMT9β, and H4K12me1 at the promoter of 3,239 genes (**Fig. 2E**). Intersection of these 3,239 targets with the 5,882 differentially expressed genes observed for AOM/DSS tumor organoids #3 uncovered 1,168 differentially expressed, direct KMT9 target genes (**Fig. 2G**). GSEA of the direct KMT9 targets revealed a significant enrichment of terms related to cell cycle (**Fig. 2H**). For instance, direct target genes with promoter presence of KMT9α, KMT9β, and H4K12me1 included cell-cycle regulators described above such as *Aurkb*, *Mcm6*, *Prr11*, *Rad51c*, and *Rpa2* (**Fig. 2I** and **C**; Supplementary Fig. S2A). Importantly, global transcriptome analysis performed from whole colorectal tumor tissue obtained from AOM/DSS–treated
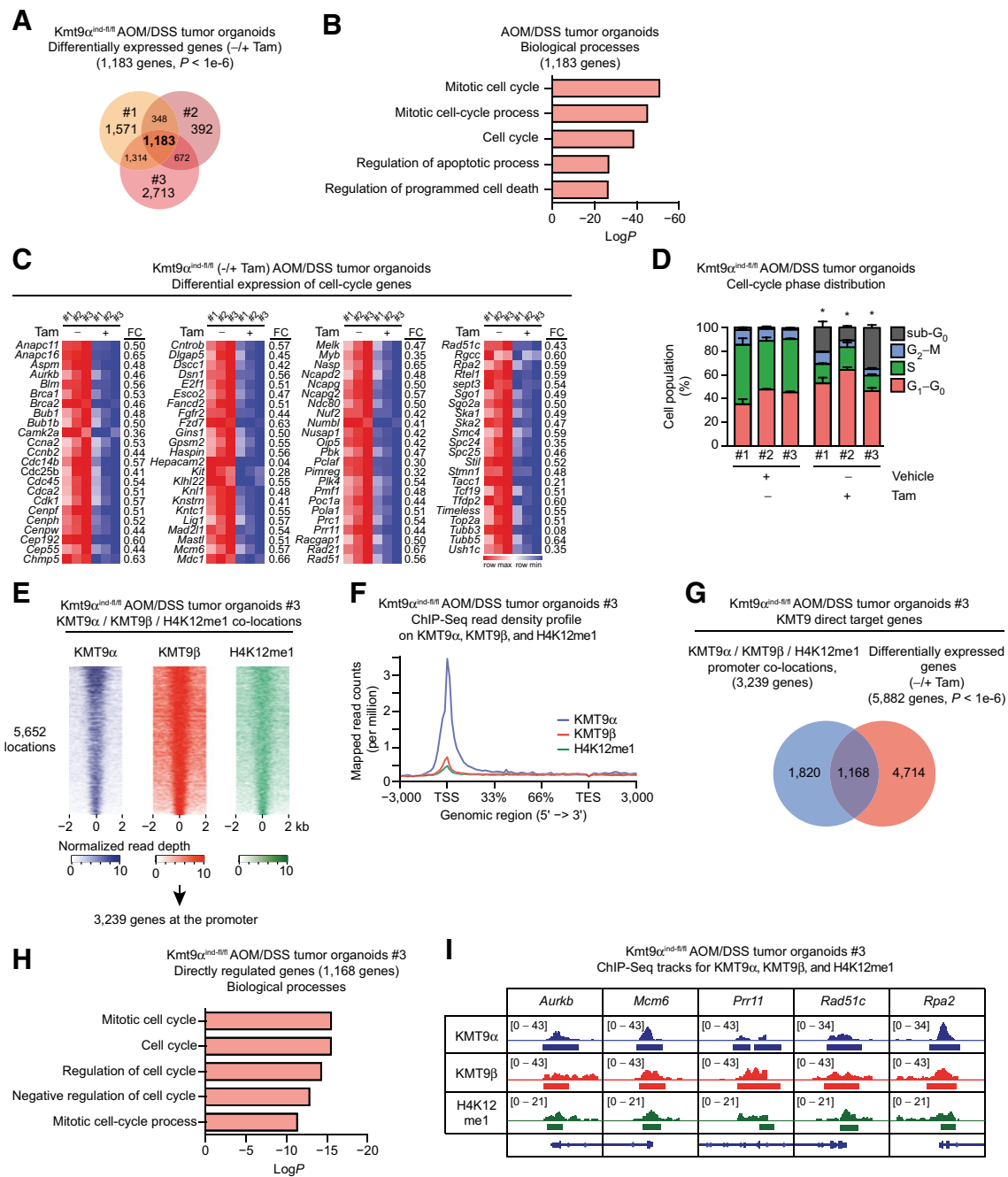
Figure 2.
KMT9α controls expression of cell-cycle genes in AOM/DSS tumors and organoids. **A,** Intersection of genes differentially expressed in Kmt9α[ind-fl/fl] AOM/DSS tumor organoid cultures (#1, #2, and #3) upon KMT9α depletion induced by tamoxifen ($P < 1e^{-6}$). **B,** Enriched biological processes obtained for the 1,183 common differentially expressed genes in AOM/DSS tumor organoids #1, #2, and #3. **C,** Heatmap showing the differential expression of genes involved in cell-cycle regulation upon KMT9α depletion from three individual AOM/DSS tumor organoid cultures. FC, fold change. **D,** Cell-cycle distribution of the three separate Kmt9α[ind-fl/fl] AOM/DSS tumor organoid cultures in the presence of vehicle or tamoxifen. Cell-cycle phases were determined by flow cytometry using BrdU incorporation and 7-AAD staining. $n = 3$ independent experiments. Data represent ± SEM. *, $P < 0.05$; two-tailed Student t test. **E,** Heatmaps of ChIP-seq read density for the 5,652 KMT9α, KMT9β, and H4K12me1 colocations observed in AOM/DSS tumor organoids #3. **F,** Average KMT9α, KMT9β, and H4K12me1 ChIP-seq read density profiles in AOM/DSS tumor organoids #3. **G,** Direct KMT9 target genes (1,168) identified by comparing genes with KMT9α, KMT9β, and H4K12me1 localized at promoter regions to differentially expressed genes upon KMT9α depletion. **H,** Enriched biological processes obtained for the direct KMT9 target genes. **I,** ChIP-seq tracks showing the presence of KMT9α, KMT9β, and H4K12me1 at promoters of representative genes in AOM/DSS tumor organoids #3. *, $P < 0.05$. Tam, tamoxifen.

Berlin et al.
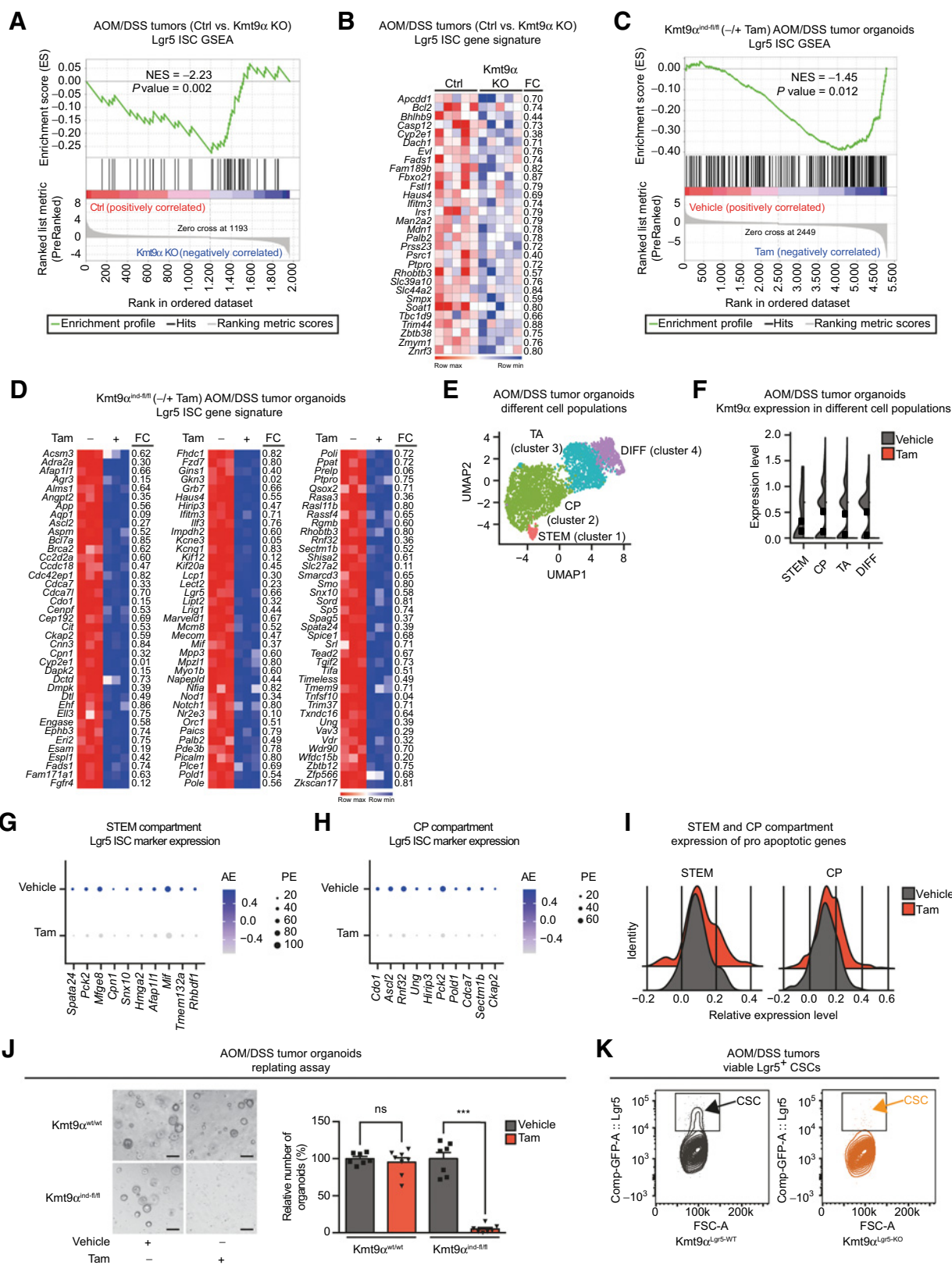
Kmt9α[IEC-WT] and Kmt9α[IEC-KO] mice also revealed cell-cycle regulation by KMT9, which is consistent with our data obtained from AOM/DSS organoids (Supplementary Fig. S2G and S2H). Together, our data show that KMT9 directly controls cell-cycle progression with a concomitant control of apoptotic state.

KMT9α controls stemness and stem cell maintenance in AOM/DSS tumors and organoids

CSCs are essential for tumor initiation and maintenance, and thereby responsible for tumor relapse and treatment failure in patients with colorectal cancer (7, 39). To investigate whether KMT9α depletion would impact CSC function, we analyzed the expression of intestinal stem cell markers in AOM/DSS tumors from Kmt9α[IEC-WT] and Kmt9α[IEC-KO] mice using a previously described Lgr5 intestinal stem cell (ISC) signature (40). GSEA revealed significant negative enrichment of the intratumoral ISC signature upon loss of KMT9α (Fig. 3A). Indeed, a total of 30 ISC-related genes were significantly downregulated in KMT9α-depleted compared with KMT9α-proficient tumors, notably Apcdd1, Dach1, and Rhobtb3, which are previously described regulators of stemness in colorectal cancer (Fig. 3B; refs. 41–43). Importantly, GSEA performed on vehicle- and tamoxifen-treated Kmt9α[ind-fl/fl] AOM/DSS tumor organoids also uncovered a negative enrichment of the Lgr5 signature with 117 stem cell–related genes significantly downregulated upon KMT9α depletion (Fig. 3C and D). To elucidate the transcriptomic underpinnings of KMT9 function in the CSC population, we performed scRNA-seq on Kmt9α[ind-fl/fl] AOM/DSS tumor organoids cultured in the presence of EtOH (vehicle) or tamoxifen. Using a droplet-based microfluidics platform, we obtained 2,340 KMT9α-proficient and 1,303 KMT9α-deficient cells after quality filtering (Supplementary Fig. S3A–S3D). By performing unsupervised clustering and two-dimensional embedding using uniform manifold approximation and projection (UMAP), we identified four tumor cell subpopulations based on the expression of established marker genes (11, 40, 44, 45) and the differentiation states by pseudotime analysis: a "stem cell" (STEM) population (cluster 1), "cycling progenitor" (CP) population (cluster 2), a "transit-amplifying" (TA) cell population (cluster 3), and a "differentiated" (DIFF) cell population (cluster 4; Fig. 3E; Supplementary Fig. S3E–S3L). Population-dependent gene expression analyses showed ubiquitous Kmt9α mRNA expression in all four cell populations and marked decrease in Kmt9α mRNA in KMT9α-deficient cells relative to KMT9α-proficient cells (Fig. 3F). Analysis of the cycle phase distribution based on the expression of cell-cycle marker genes (Supplementary Fig. S3M) was in agreement with the role of KMT9α in cell-cycle regulation described above (Fig. 2D). Furthermore, in accordance with the bulk RNA-seq data, we observed downregulation of essential S-phase genes such as Mcm6 and Rpa2 by scRNA-seq upon KMT9α depletion (Supplementary Fig. S3N). Interestingly, numerous stem cell–related genes listed in the previously described Lgr5+ ISC signature (40) were downregulated upon loss of KMT9α in both precursor populations (Fig. 3G and H). In addition, we observed increased expression of proapoptotic genes in KMT9α-deficient STEM and CP populations, emphasizing the relevant role of KMT9 in tumoral stem cell maintenance (Fig. 3I; Supplementary Table S3). These data suggest that loss of KMT9α might affect the self-renewal potential and colony formation capacity of tumor stem/initiating cells. To test this hypothesis, single cells isolated from KMT9α-proficient and deficient AOM/DSS tumor organoids were evaluated for anchorage-independent sphere formation in a secondary replating assay. Importantly, the secondary sphere formation capacity of cells derived from KMT9α-deficient organoids was blocked (Fig. 3J).

To corroborate these findings in vivo, we crossed Kmt9α^{fl/fl} mice with the Lgr5-EGFP-IRES-CreERT2 deleter strain (11) for tamoxifen-inducible selective Kmt9α ablation in intestinal Lgr5+ stem cells. Tamoxifen-treated mice were challenged with AOM/DSS and Lgr5-expressing CSCs were intratumorally traced in vivo using enhanced green fluorescent protein (EGFP) reporter. In accordance with our hypothesis, we found that the percentage of viable Lgr5-EGFP–positive (Lgr5-EGFP+) CSCs was markedly decreased upon Kmt9α loss in the collected tumors (Fig. 3K). All together, our data demonstrate the importance of KMT9 in maintaining the self-renewal potential and viability of tumor stem/initiating cells.

KMT9α is a potential therapeutic target for the treatment of colorectal cancer

Besides inflammation-induced colorectal tumorigenesis, sporadic colorectal cancer results from the progressive accumulation of genetic and epigenetic alterations (3, 46). To investigate whether KMT9 loss also affects sporadic colorectal carcinogenesis driven by key human colorectal cancer mutations, we generated epithelial tumor organoids from Apc^{fl/fl} p53^{fl/fl} Kras[G12D/+] Kmt9α^{fl/fl} and Apc^{fl/fl} p53^{fl/fl} Kras[G12D/+] Kmt9α^{+/+} mice. Transduction of organoids with cre-expressing adenovirus resulted in APKK (Apc[KO]/p53[KO]/Kras[G12D]/Kmt9α[KO]) and APK (Apc[KO]/p53[KO]/Kras[G12D]/Kmt9α[WT]) colorectal cancer organoids. In line with our results presented above, we observed a severe impairment in growth for KMT9α-deficient APKK organoids in comparison with KMT9α-proficient APK colorectal cancer organoids (Fig. 4A), suggesting a critical role for KMT9 in sporadic tumor progression. To unravel the mechanistic role of KMT9α in sporadic colorectal cancer, we performed RNA-seq in APK and APKK organoids. In line with our results obtained with AOM/DSS tumor organoids, we observed a significant downregulation of genes involved in cell-cycle progression in APKK organoids (Fig. 4B). Furthermore, we identified 124 stem cell–related genes significantly downregulated

---

Figure 3.

KMT9α controls stemness and stem cell maintenance in AOM/DSS tumors and organoids. **A,** GSEA of differentially expressed genes in AOM/DSS tumors from Kmt9α[IEC-KO] compared with tumors from Kmt9α[IEC-WT] mice uncovered significant negative enrichment of the Lgr5 ISC gene signature. **B,** Heatmap showing reduced expression of stem cell–related genes upon KMT9α loss in AOM/DSS tumors. **C,** GSEA of differentially expressed genes in AOM/DSS tumor organoids #3 (vehicle vs. tamoxifen). **D,** Heatmap showing mRNA levels of stem cell–related genes significantly downregulated by KMT9α depletion in AOM/DSS tumor organoids. FC, fold change; $P < 1e^{-6}$. **E,** UMAP plot showing the four subpopulations, stem cells (STEM; cluster 1), cycling progenitor cells (CP; cluster 2), transit-amplifying cells (TA; cluster 3), and differentiated cells (DIFF; cluster 4) identified in vehicle-treated Kmt9α[ind-fl/fl] AOM/DSS tumor organoids by scRNA-seq. **F,** Violin plots showing Kmt9α levels in the four identified subpopulations of Kmt9α[ind-fl/fl] AOM/DSS tumor organoids following vehicle or tamoxifen treatment. **G** and **H,** Dot plot of the top 10 stem cell–related genes downregulated by KMT9α depletion in the STEM (**G**) and CP (**H**) populations of AOM/DSS tumor organoids. PE, percent expressed; AE, average expression. **I,** Ridge plot representing the relative expression of proapoptotic genes in vehicle- and tamoxifen-treated Kmt9α[ind-fl/fl] STEM and CP populations. **J,** Representative images of the secondary organoid-forming capacity of AOM/DSS tumor Kmt9α[wt/wt] (Ctrl) and Kmt9α[ind-fl/fl] (#3) organoids in the presence of vehicle or tamoxifen (left). Scale bars, 400 μm. Right, relative number of secondary organoids after replating normalized to vehicle-treated organoids. Data represent ±SEM. ns, not significant; ***, $P < 0.001$; two-tailed unpaired t test. **K,** Contour plots depicting viable EGFP+/Lgr5+ stem cells in AOM/DSS tumors from Kmt9α[Lgr5-WT] (n = 4) and Kmt9α[Lgr5-KO] (n = 4) mice. Tam, tamoxifen.
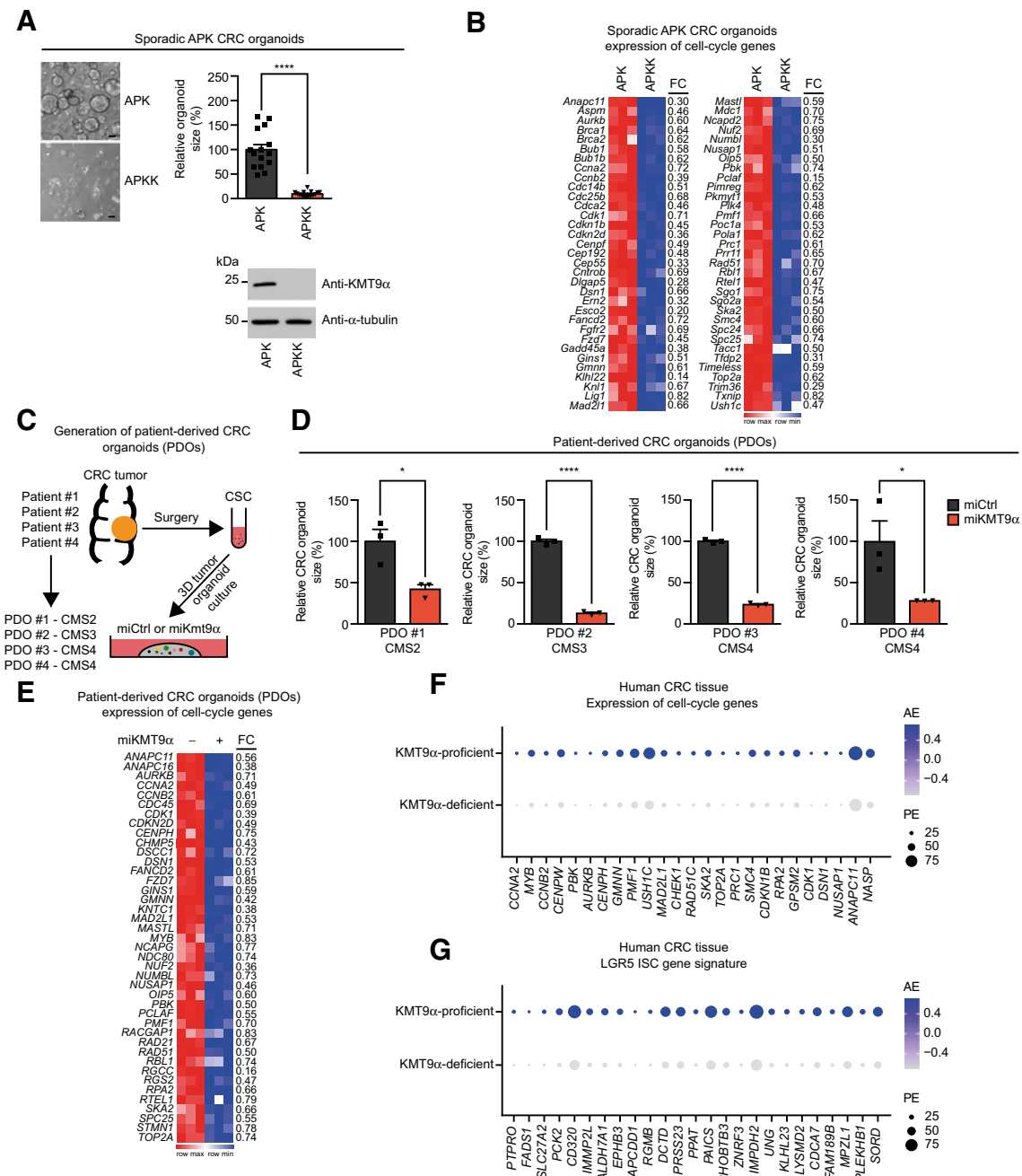
Berlin et al.

Figure 4.
KMT9α is a potential therapeutic target for the treatment of colorectal cancer. **A,** Representative pictures of APK (Apc^{KO}/p53^{KO}/Kras^{G12D}/Kmt9α^{WT}) and APKK (Apc^{KO}/p53^{KO}/Kras^{G12D}/Kmt9α^{KO}) tumor organoids. Scale bars, 50 μm (left). Top right, normalized size of APK and APKK tumor organoids. Bottom right, Western blot showing the expression of KMT9α in APK and APKK tumor organoids. **B,** Heatmap showing significantly downregulated genes involved in cell-cycle progression in APK compared with APKK tumor organoids. FC, fold change; $P < 1e^{-6}$. **C,** PDOs were developed from colorectal cancer tumors of individual patients (#1, #2, #3, #4) covering CMS2–4 and transduced with lentivirus encoding either control miRNA (miCtrl) or miRNA directed against *KMT9α* (miKMT9α). **D,** Reductions in organoid size were observed for PDOs #1–4 upon *KMT9α* depletion by miKMT9α relative to miCtrl. All data represent means ± SEM. *, $P < 0.05$; ****, $P < 0.0001$; two-tailed Student t test. **E,** Heatmap showing significantly downregulated cell-cycle genes in PDOs. FC, fold change; $P < 1e^{-6}$. **F** and **G,** Tumor epithelial cell population from a previously published single-cell RNA-seq dataset from a cohort of 23 Korean patients with colorectal cancer stratified by *KMT9α* expression. Dot plot showing the top 25 cell-cycle genes (**F**) and stem cell–related genes (**G**) downregulated in KMT9α-deficient epithelial colorectal cancer cells compared with KMT9α-proficient cells. AE, average expression; CRC, colorectal cancer; PE, percent expressed.

by KMT9α depletion (Supplementary Fig. S4A). To corroborate our data in human colorectal tumors, we established patient-derived organoid (PDO) cultures from four patients with colorectal cancer (PDO #1, #2, #3, and #4) representing CMS2, CMS3, and CMS4 tumors (**Fig. 4C**). We did not consider CMS1 tumors due to the low expression levels of *KMT9α* in CMS1 compared with CMS2–4 tumor samples (Supplementary Fig. S1A). Human PDOs were transduced with lentivirus driving expression of either control miRNA (miCtrl) or miRNA directed against *KMT9α* (miKMT9α) and organoid growth was analyzed *in vitro*. Importantly, *KMT9α* knockdown efficiently reduced tumor organoid size in all investigated PDOs (**Fig. 4D**; Supplementary Fig. S4B and S4C). Consistent with this morphologic phenotype, transcriptomic analysis of the PDOs revealed a significant downregulation of genes involved in cell-cycle progression (**Fig. 4E**), as well as downregulation of multiple genes involved in CSC function of colorectal cancer (Supplementary Fig. S4D), thus corroborating the results obtained in murine inflammation-induced and sporadic colorectal tumorigenesis. We next investigated the function of KMT9α in the epithelial compartment of primary tumor tissue from patients with colorectal cancer. We analyzed single-cell transcriptome data from 23 Korean patients with colorectal cancer (GSE132435) and stratified epithelial tumor cells in KMT9α-proficient and KMT9α-deficient cell populations (Supplementary Fig. S4E; ref. 47). Interestingly, most of the genes involved in cell-cycle progression and genes downregulated upon depletion of KMT9α in murine AOM/DSS and in sporadic murine colorectal cancer organoids, were also downregulated in human epithelial KMT9α-deficient colorectal cancer cells (**Fig. 4F**). Furthermore, we analyzed the LGR5 ISC gene signature (40) and found numerous signature genes downregulated in epithelial KMT9α-deficient human colorectal cancer cells (**Fig. 4G**).

Together, these findings demonstrate a decisive role of KMT9α in mouse and human sporadic colorectal carcinogenesis and as well as in inflammation-induced tumorigenesis, thereby identifying inhibition of KMT9 as a highly promising single-target approach for the treatment of colorectal cancer.

Discussion

In this study, we used mouse models and tumor organoids derived from mice and human patients as well as human tumor tissue to uncover an essential role of KMT9, a novel H4K12me1 histone methyltransferase, in colorectal cancer. Our data show that growth of inflammation-induced tumors as well as sporadic colorectal cancer is dramatically reduced in the absence of KMT9α *in vitro* and *in vivo*. While we cannot exclude that additional KMT9 functions could potentially contribute to the observed phenotype, we demonstrate that a major consequence of KMT9 loss is the impairment of tumor growth via disrupting the regulation of genes involved in proliferation, cell-cycle progression, and apoptosis. So far, we cannot fully rule out the possibility that the loss of KMT9 is playing a role in the inflammatory or regenerative process after AOM/DSS treatment, which warrants further investigation. Moreover, we have also demonstrated that KMT9α ablation impairs tumor growth in CMS2-, CMS3-, and CMS4 PDOs. To date, it is well accepted that the interpatient heterogeneity of colorectal cancer has clinical implications on therapeutic responses (48). Thus, future investigations have to examine different colorectal cancer subtypes for their responsiveness to targeting KMT9 *in vivo*.

Besides reduction of tumor growth, elimination of colorectal CSCs to prevent tumor recurrence and metastasis remains one of the biggest clinical challenges in treating colorectal cancer. To date, most therapeutic strategies rely on combination therapy of a CSC-targeting agent with eradication of tumor mass (49), where targeting of CSCs is hindered due to its similarity with benign, noncancerous stem cells. In this study, we showed that in addition to a major impact on inhibiting tumor growth, targeting KMT9 also downregulated numerous stem cell–related genes and impaired CSC function and maintenance. Thus, inhibition of KMT9 in colorectal cancer may be a promising therapy to target colorectal CSCs.

Currently, the use of epigenetic drugs as monotherapy for colorectal cancer have largely failed to improve patient outcomes (50, 51). The main issues leading to the failure of these epigenetic agents include intratumor and interpatient heterogeneity and the essential function of epigenetic regulators in both malignant and benign cells. Importantly, we found that without AOM/DSS insult, mice with specific KMT9α ablation in intestinal epithelial cells survive without a noticeable phenotype and do not exhibit morphologic changes of the colon tissue. Thus, weak side effects of KMT9 targeting would be assumed in the clinical context. In consequence, the development of small-molecule inhibitors targeting KMT9 might be a promising therapeutic avenue for colorectal cancer treatment.

Authors' Contributions

C. Berlin: Conceptualization, data curation, formal analysis, validation, investigation, methodology, writing–original draft. **F. Cottard:** Conceptualization, data curation, formal analysis, validation, investigation, methodology, writing–original draft. **D. Willmann:** Data curation, software, formal analysis. **S. Urban:** Investigation, methodology. **S.M. Tirier:** Data curation, software, formal analysis. **L. Marx:** Investigation. **K. Rippe:** Resources, methodology. **M. Schmitt:** Investigation, methodology. **V. Petrocelli:** Investigation, methodology. **F.R. Greten:** Conceptualization. **S. Fichtner-Feigl:** Conceptualization. **R. Kesselring:** Conceptualization, resources, investigation, methodology. **E. Metzger:** Conceptualization, writing–original draft. **R. Schüle:** Conceptualization, supervision, funding acquisition, writing–original draft.

References

1. Siegel RL, Miller KD, Jemal A. Cancer statistics, 2019. CA Cancer J Clin 2019;69: 7–34.
2. Kuipers EJ, Grady WM, Lieberman D, Seufferlein T, Sung JJ, Boelens PG, et al. Colorectal cancer. Nat Rev Dis Primers 2015;1:15065.
3. Guinney J, Dienstmann R, Wang X, de Reynies A, Schlicker A, Soneson C, et al. The consensus molecular subtypes of colorectal cancer. Nat Med 2015; 21:1350–6.
4. Dienstmann R, Vermeulen L, Guinney J, Kopetz S, Tejpar S, Tabernero J. Consensus molecular subtypes and the evolution of precision medicine in colorectal cancer. Nat Rev Cancer 2017;17:79–92.
5. Berg KCG, Eide PW, Eilertsen IA, Johannessen B, Bruun J, Danielsen SA, et al. Multi-omics of 34 colorectal cancer cell lines - a resource for biomedical studies. Mol Cancer 2017;16:116.
6. Linnekamp JF, Hooff SRV, Prasetyanti PR, Kandimalla R, Buikhuisen JY, Fessler E, et al. Consensus molecular subtypes of colorectal cancer are recapitulated in in vitro and in vivo models. Cell Death Differ 2018;25: 616–33.
7. Ahmed M. Colon cancer: a clinician's perspective in 2019. Gastroenterology Res 2020;13:1–10.
8. Duineveld LA, van Asselt KM, Bemelman WA, Smits AB, Tanis PJ, van Weert HC, et al. Symptomatic and asymptomatic colon cancer recurrence: A Multi-center Cohort Study. Ann Fam Med 2016;14:215–20.
9. Lytle NK, Barber AG, Reya T. Stem cell fate in cancer growth, progression and therapy resistance. Nat Rev Cancer 2018;18:669–80.
10. Morgan RG, Mortensson E, Williams AC. Targeting LGR5 in Colorectal Cancer: therapeutic gold or too plastic? Br J Cancer 2018;118:1410–18.
11. Barker N, van Es JH, Kuipers J, Kujala P, van den Born M, Cozijnsen M, et al. Identification of stem cells in small intestine and colon by marker gene Lgr5. Nature 2007;449:1003–7.
12. Kemper K, Prasetyanti PR, De Lau W, Rodermond H, Clevers H, Medema JP. Monoclonal antibodies against Lgr5 identify human colorectal cancer stem cells. Stem Cells 2012;30:2378–86.
13. Hirsch D, Barker N, McNeil N, Hu Y, Camps J, McKinnon K, et al. LGR5 positivity defines stem-like cells in colorectal cancer. Carcinogenesis 2014;35: 849–58.
14. Zeuner A, Todaro M, Stassi G, De Maria R. Colorectal cancer stem cells: from the crypt to the clinic. Cell Stem Cell 2014;15:692–705.
15. Medema JP. Targeting the Colorectal Cancer Stem Cell. N Engl J Med 2017;377: 888–90.
16. Vaiopoulos AG, Athanasoula KC, Papavassiliou AG. Epigenetic modifications in colorectal cancer: molecular insights and therapeutic challenges. Biochim Biophys Acta 2014;1842:971–80.
17. Chen Y, Ren B, Yang JS, Wang HY, Yang G, Xu RY, et al. The role of histone methylation in the development of digestive cancers: a potential direction for cancer management. Signal Transduct Target Ther 2020;5:143.
18. Jung G, Hernandez-Illan E, Moreira L, Balaguer F, Goel A. Epigenetics of colorectal cancer: biomarker and therapeutic potential. Nat Rev Gastro Hepat 2020;17:111–30.
19. Greer EL, Shi Y. Histone methylation: a dynamic mark in health, disease and inheritance. Nat Rev Genet 2012;13:343–57.
20. Huang T, Lin C, Zhong LL, Zhao L, Zhang G, Lu A, et al. Targeting histone methylation for colorectal cancer. Therap Adv Gastroenterol 2017; 10:114–31.
21. Salz T, Li G, Kaye F, Zhou L, Qiu Y, Huang S. hSETD1A regulates Wnt target genes and controls tumor growth of colorectal cancer cells. Cancer Res 2014;74: 775–86.
22. Metzger E, Wang S, Urban S, Willmann D, Schmidt A, Offermann A, et al. KMT9 monomethylates histone H4 lysine 12 and controls proliferation of prostate cancer cells. Nat Struct Mol Biol 2019;26:361–71.
23. Baumert HM, Metzger E, Fahrner M, George J, Thomas RK, Schilling O, et al. Depletion of histone methyltransferase KMT9 inhibits lung cancer cell proliferation by inducing non-apoptotic cell death. Cancer Cell Int 2020; 20:52.
24. Eide PW, Bruun J, Lothe RA, Sveen A. CMScaller: an R package for consensus molecular subtyping of colorectal cancer pre-clinical models. Sci Rep 2017;7: 16618.
25. Sato T, Stange DE, Ferrante M, Vries RG, Van Es JH, Van den Brink S, et al. Long-term expansion of epithelial organoids from human colon, adenoma, adenocarcinoma, and Barrett's epithelium. Gastroenterology 2011;141: 1762–72.
26. Metzger E, Wissmann M, Yin N, Muller JM, Schneider R, Peters AH, et al. LSD1 demethylates repressive histone marks to promote androgen-receptor-dependent transcription. Nature 2005;437:436–9.
27. Langmead B, Salzberg SL. Fast gapped-read alignment with Bowtie 2. Nat Methods 2012;9:357–9.
28. Zhang Y, Liu T, Meyer CA, Eeckhoute J, Johnson DS, Bernstein BE, et al. Model-based analysis of ChIP-Seq (MACS). Genome Biol 2008;9:R137.
29. Thorvaldsdottir H, Robinson JT, Mesirov JP. Integrative Genomics Viewer (IGV): high-performance genomics data visualization and exploration. Brief Bioinform 2013;14:178–92.
30. Heinz S, Benner C, Spann N, Bertolino E, Lin YC, Laslo P, et al. Simple combinations of lineage-determining transcription factors prime cis-regulatory elements required for macrophage and B cell identities. Mol Cell 2010;38:576–89.
31. Fachal L, Aschard H, Beesley J, Barnes DR, Allen J, Kar S, et al. Fine-mapping of 150 breast cancer risk regions identifies 191 likely target genes. Nat Genet 2020; 52:56–73.
32. Dobin A, Davis CA, Schlesinger F, Drenkow J, Zaleski C, Jha S, et al. STAR: ultrafast universal RNA-seq aligner. Bioinformatics 2013;29:15–21.
33. Robinson SJ, Parkin IA. Differential SAGE analysis in Arabidopsis uncovers increased transcriptome complexity in response to low temperature. BMC Genomics 2008;9:434.
34. Chandrashekar DS, Bashel B, Balasubramanya SAH, Creighton CJ, Ponce-Rodriguez I, Chakravarthi B, et al. UALCAN: A Portal for Facilitating Tumor Subgroup Gene Expression and Survival Analyses. Neoplasia 2017;19:649–58.
35. Hameyer D, Loonstra A, Eshkind L, Schmitt S, Antunes C, Groen A, et al. Toxicity of ligand-dependent Cre recombinases and generation of a conditional Cre deleter mouse allowing mosaic recombination in peripheral tissues. Physiol Genomics 2007;31:32–41.
36. Parang B, Barrett CW, Williams CS. AOM/DSS model of Colitis-Associated cancer. Methods Mol Biol 2016;1422:297–307.
37. De Robertis M, Massi E, Poeta ML, Carotti S, Morini S, Cecchetelli L, et al. The AOM/DSS murine model for the study of colon carcinogenesis: From pathways to diagnosis and therapy studies. J Carcinog 2011;10:9.
38. el Marjou F, Janssen KP, Chang BH, Li M, Hindie V, Chan L, et al. Tissue-specific and inducible Cre-mediated recombination in the gut epithelium. Genesis 2004; 39:186–93.
39. Nassar D, Blanpain C. Cancer stem cells: Basic concepts and therapeutic implications. Annu Rev Pathol 2016;11:47–76.
40. Munoz J, Stange DE, Schepers AG, van de Wetering M, Koo BK, Itzkovitz S, et al. The Lgr5 intestinal stem cell signature: robust expression of proposed quiescent '+4' cell markers. EMBO J 2012;31:3079–91.
41. de Sousa E, Melo F, Colak S, Buikhuisen J, Koster J, Cameron K, et al. Methylation of cancer-stem-cell-associated Wnt target genes predicts poor prognosis in colorectal cancer patients. Cell Stem Cell 2011;9:476–85.
42. Fevr T, Robine S, Louvard D, Huelsken J. Wnt/beta-catenin is essential for intestinal homeostasis and maintenance of intestinal stem cells. Mol Cell Biol 2007;27:7551–9.
43. Hu X, Zhang L, Li Y, Ma X, Dai W, Gao X, et al. Organoid modelling identifies that DACH1 functions as a tumour promoter in colorectal cancer by modulating BMP signalling. EBioMedicine 2020;56:102800.
44. Takeda K, Mizushima T, Yokoyama Y, Hirose H, Wu X, Qian Y, et al. Sox2 is associated with cancer stem-like properties in colorectal cancer. Sci Rep 2018;8: 17639.
45. Wiener Z, Hogstrom J, Hyvonen V, Band AM, Kallio P, Holopainen T, et al. Prox1 promotes expansion of the colorectal cancer stem cell population to fuel tumor growth and ischemia resistance. Cell Rep 2014;8:1943–56.
46. Fearon ER, Vogelstein B. A genetic model for colorectal tumorigenesis. Cell 1990; 61:759–67.
47. Lee H-O, Hong Y, Etlioglu HE, Cho YB, Pomella V, Van den Bosch B, et al. Lineage-dependent gene expression programs influence the immune landscape of colorectal cancer. Nat Genet 2020;52:594–603.
48. Molinari C, Marisi G, Passardi A, Matteucci L, De Maio G, Ulivi P. Heterogeneity in colorectal cancer: a challenge for personalized medicine? Int J Mol Sci 2018;19:3733.
49. Kaiser J. The cancer stem cell gamble. Science 2015;347:226–9.
50. Vincent A, Ouelkdite-Oumouchal A, Souidi M, Leclerc J, Neve B, Van Seuningen I. Colon cancer stemness as a reversible epigenetic state: implications for anticancer therapies. World J Stem Cells 2019;11:920–36.
51. Baretti M, Azad NS. The role of epigenetic therapies in colorectal cancer. Curr Prob Cancer 2018;42:530–47.

Cancer Research

The Journal of Cancer Research (1916–1930) | The American Journal of Cancer (1931–1940)

AAC-R American Association
for Cancer Research

KMT9 Controls Stemness and Growth of Colorectal Cancer

Christopher Berlin, Félicie Cottard, Dominica Willmann, et al.

Updated version	Access the most recent version of this article at: doi:10.1158/0008-5472.CAN-21-1261
Supplementary Material	Access the most recent supplemental material at: http://cancerres.aacrjournals.org/content/suppl/2021/11/04/0008-5472.CAN-21-1261.DC1

Cited articles	This article cites 51 articles, 5 of which you can access for free at: http://cancerres.aacrjournals.org/content/82/2/210.full#ref-list-1

E-mail alerts	Sign up to receive free email-alerts related to this article or journal.
Reprints and Subscriptions	To order reprints of this article or to subscribe to the journal, contact the AACR Publications Department at pubs@aacr.org.
Permissions	To request permission to re-use all or part of this article, use this link http://cancerres.aacrjournals.org/content/82/2/210. Click on "Request Permissions" which will take you to the Copyright Clearance Center's (CCC) Rightslink site.